



**University of Murcia**

PHYSICS DEGREE

2022/2023

**Graphene Oxide and  
Reduced Graphene Oxide:  
Electronic properties**

*Faculty of Chemistry*

Author:

Ginés González Guirado

Tutors:

Elisa Palacios Lidón and Mario Navarro Rodríguez



## DECLARACIÓN DE ORIGINALIDAD

D. Ginés González Guirado, estudiante del Grado en Física de la Facultad de Química de la Universidad de Murcia, **DECLARO:**

Que el Trabajo de Fin de Grado que presento para su exposición y defensa titulado  
**GRAPHENE OXIDE AND REDUCED GRAPHENE OXIDE: ELECTRONIC PROPERTIES**  
y cuyo/s tutor/es es/son

Dña. Elisa Palacios Lidón

D. Mario Navarro Rodríguez

es original y que todas las fuentes utilizadas para su realización han sido debidamente citadas en el mismo.

Murcia, a 18 de junio de 2023

Firma

## Abstract

Graphene oxide (GO) is a two-dimensional disordered material with oxygen-containing functional groups randomly distributed in the basal plane. When part of its functional groups are eliminated, through reduction, its properties change and it is called reduced graphene oxide (rGO). Because their electronic and optical properties can be controlled by removing functional groups, the range of applications for which they can be used, in electronic devices, is very wide. The advancement of using GO and rGO in various applications relies heavily on understanding their electronic structure at the nanoscale. However, obtaining direct experimental insights is difficult due to the inherent disorder of these materials.

The aim of this work is to analyze the electronic properties of individual monolayer flakes of GO and rGO. To achieve this, an Atomic Force Microscope (AFM) has been utilized. The AFM allows the visualization of material surfaces with nanometer resolution, while also providing information about the nanoscale electronic properties of the material through Kelvin Probe Force Microscopy (KPFM). Measurements were conducted in controlled humidity to avoid the presence of a water layer on surfaces, which could interfere with the signal from the studied materials.

It has been seen that GO presents the existence of localized charge domains, while the observed surface potential in rGO is uniform, indicating that conduction is greater in rGO. Through a charge injection experiment, it has been verified that in rGO the charge propagates much faster than in GO, evidencing the conductive nature of rGO and the insulating nature of GO.

## Resumen

El óxido de grafeno (GO) es un material desordenado bidimensional con grupos funcionales que contienen oxígeno distribuidos aleatoriamente en el plano basal. Cuando se eliminan parte de sus grupos funcionales, por reducción, sus propiedades cambian y se denomina óxido de grafeno reducido (rGO). Debido a que sus propiedades electrónicas y ópticas se pueden controlar mediante la eliminación de grupos funcionales, la gama de aplicaciones para las que se pueden utilizar en dispositivos electrónicos es muy amplia. El avance del uso de GO y rGO en diversas aplicaciones depende en gran medida de la comprensión de su estructura electrónica a nanos escala. Sin embargo, obtener conocimientos experimentales directos es difícil debido al desorden inherente de estos materiales.

El objetivo de este trabajo es analizar las propiedades electrónicas de láminas monocapa individuales de GO y rGO. Para lograr esto, se ha utilizado un Microscopio de Fuerza Atómica (AFM). El AFM permite la visualización de superficies de materiales con resolución nanométrica, al mismo tiempo que proporciona información sobre las propiedades electrónicas a nanos escala del material a través de la técnica Kelvin Probe Force Microscopy (KPFM). Las mediciones se realizaron en condiciones de humedad controlada, para evitar la presencia de una capa de agua en las superficies, que podría interferir con la señal de los materiales estudiados.

Se ha visto que GO presenta la existencia de dominios de carga localizados, mientras que el potencial de superficie observado en rGO es uniforme, lo que indica que la conducción es mayor en rGO. Mediante un experimento de inyección de carga se ha comprobado que en rGO la carga se propaga mucho más rápido que en GO, evidenciando el carácter conductor de rGO y el carácter aislante de GO.

# Contents

<b>1</b>	<b>Introduction</b>	<b>1</b>
<b>2</b>	<b>Graphene Oxide and rGO</b>	<b>2</b>
2.1	Structure of GO and rGO. . . . .	2
2.2	Methods of reduction. . . . .	3
2.2.1	Chemical reduction with hydrazine. . . . .	3
2.2.2	Thermal reduction. . . . .	3
2.3	Properties of GO and rGO. . . . .	4
2.4	Applications of GO and rGO. . . . .	6
<b>3</b>	<b>Surface physics and Atomic Force Microscopy.</b>	<b>8</b>
3.1	Work function of a solid and surface potential. . . . .	8
3.2	The fundamentals of the Atomic Force Microscope (AFM). . . . .	10
3.3	Kelvin Probe Force Microscopy (KPFM). . . . .	12
<b>4</b>	<b>Experimental results.</b>	<b>15</b>
4.1	Preparation of the sample. . . . .	15
4.2	Monolayer GO on SiO <sub>2</sub> substrate. . . . .	15
4.2.1	Topography and KPFM of monolayer GO . . . . .	15
4.3	Flakes of rGO on SiO <sub>2</sub> substrate. . . . .	16
4.3.1	Topography and KPFM of rGO flakes. . . . .	16
4.4	Charge injection. . . . .	17
4.5	Comparison GO and rGO on SiO <sub>2</sub> substrate. . . . .	19
<b>5</b>	<b>Conclusions and future.</b>	<b>21</b>
<b>References</b>		<b>22</b>
<b>Appendix</b>		<b>24</b>

# 1 Introduction

Graphene is a perfectly ordered two-dimensional (2D) material forming a honeycomb lattice with  $sp^2$  hybridized carbon atoms and one atomic layer thick [1]. Its properties have been widely studied, since its discovery by Novoselov et al [2] in 2004. Thus, it has been proven that it has phenomenal mechanical properties for use in devices of different types, which arise predominantly from the establishment of  $\sigma$  bonds between overlapping  $sp^2$  orbitals in the basal plane [3]. In addition, its electronic properties, characterized by a zero band gap, arise fundamentally from the formation of  $\pi$ -bonds between the  $p_z$  orbitals perpendicular to the basal plane [3]. This makes electrons behave as massless relativistic fermions satisfying the Dirac equation [4].

Graphene oxide (GO) is a 2D disordered, amorphous and heterogeneous material with oxygen-containing functional groups randomly distributed in the basal plane, so the hybridisation of some carbon atoms changes from  $sp^2$  to  $sp^3$ . Therefore, there are not  $\pi$ -bonds and the properties of GO are very different from those of graphene [1]. GO began to be studied in depth to try to obtain graphene from it, due to the problem of producing graphene on a large scale. In addition its physical and chemical properties can be modified by removing part of the functional groups from its basal plane, through the so-called reduction methods to obtain reduced graphene oxide (rGO). RGO is still a disordered and inhomogeneous 2D material, however it has different properties to GO thanks to the partial recovery of the  $sp^2$  hybridization in the carbon atoms where the functional groups have been removed. Therefore, GO and rGO are not well defined materials, because their properties change easily, depending on the oxygen-containing functional groups that they contain and the way they are distributed along the lattice after the reduction process.

An advantage of GO and rGO with respect to graphene is that they are easier to synthesize, process, and integrate into devices by using existing planar thin-film-electronics techniques. Thus, they have found a wide variety of applications such as transparent conductors and gas detection among others.

The aim of this work is to characterize the electronic properties of individual GO and rGO monolayer flakes. For this purpose, it has been used an Atomic Force Microscope

(AFM). The AFM allows the visualization of material surfaces with nanometer resolution, while also providing information about the nanoscale electronic properties of the material through Kelvin Probe Force Microscopy (KPFM). Measurements have been carried out under controlled humidity conditions, since under ambient conditions, a thin layer of water is deposited on almost all surfaces, screening the signal coming from the studied materials.

## 2 Graphene Oxide and rGO

### 2.1 Structure of GO and rGO.

A GO sheet consists partially of  $sp^2$  hybridized carbon atoms and carbon atoms bonded  $sp^3$  with tetrahedral form, which are slightly displaced above or below the graphene plane, due to the oxygen-containing functional groups randomly distributed in the basal plane [1]. The oxygen-containing functional groups in the basal plane of GO are predominantly epoxies and hydroxyls, although there are also others [5].

rGO is obtained when part of the oxygen-containing functional groups are eliminated, by means of reduction methods, so that the hybridization of some carbon atoms changes from  $sp^3$  to  $sp^2$  in the atoms, where those functional groups have been removed. In Fig. 1), it is shown a depiction of the structure and composition of graphene, GO and rGO. In addition to the process to go from one to the other.

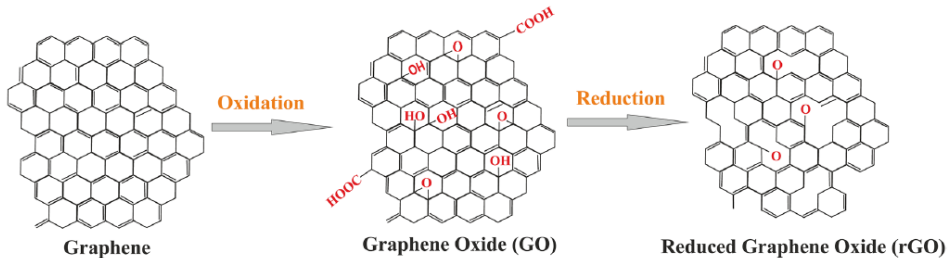


Figure 1: Left: Graphene. Center: Graphene Oxide. Right: Reduced Graphene Oxide. Adapted from [6].

## **2.2 Methods of reduction.**

To reduce GO, several reduction methods have been developed. Some of the most common ones are chemical, thermal, photo-mediated, and biological reduction. being the chemical and thermal reduction the most widely used. Among the different reducing agents, hydrazine is the most used one and the one used in this work.

### **2.2.1 Chemical reduction with hydrazine.**

For this work, the reduction of GO with hydrazine is carried out in solution. The reduction process occurs through multiple pathways. In the first pathway, Hydrazine ( $\text{NH}_2\text{NH}_2$ ) reacts with epoxy groups present on GO sheets. In the second pathway, the  $\text{NH-NH}_2$ , that formed after the previous reaction, undergoes cleavage without hydrogen abstraction, leading to the formation of hydroxyl groups. These hydroxyl groups can react with the three hydrogens in  $\text{NH-NH}_2$ , resulting in the formation of  $\text{NH-NH}$  or  $\text{N-NH}_2$  groups along with the release of water ( $\text{H}_2\text{O}$ ). These hydrazine alcohols undergo thermal dehydration, producing hydrazone by eliminating oxygen. Then, the hydrazone can experience a new reduction due to the Wolff–Kishner–Huang-type reaction, thus leaving rGO with very few functional groups [7].

The disadvantages of hydrazine reduction of GO include high toxicity, potential unintended doping with amide group or pyrazole ring, and increased costs due to residue generation on an industrial level [7].

### **2.2.2 Thermal reduction.**

Thermal reduction is a direct method to obtain rGO. The reduction temperature is chosen based on the application to which the rGO is going to be used, because the structural decomposition of the GO basal plane and the extent of reduction depend on the temperature [7].

At temperatures between 140 and 180°C, the chemisorbed water molecules are removed. If the temperature is increased between 180 and 600°C, the major carboxyl groups are eliminated. By further increasing the temperature, in the range between 600 and 800°C,

all carboxyl and some hydroxyl groups are eliminated. Moreover, if the temperature is raised to 1000°C, it leads to the elimination of the remaining hydroxyl and some epoxy groups, but it generates numerous structural defects resulting from the cracking of C=C bonds on the basal plane [7].

### 2.3 Properties of GO and rGO.

The electrical and optical properties of GO and rGO are heavily influenced by the spatial distribution of the oxygen-containing functional groups. Hence, the method of reduction is critically important to endow the material with specific properties being possible to tune it from insulating, semiconducting or semimetallic, while conserving optical transparency [1].

A difference between GO and rGO is the absorbance of the electromagnetic spectrum. When GO is suspended in water it appears yellowish, however rGO appears black and it can be seen in Fig. 2 that rGO absorbs more wavelengths, so it has a more metallic aspect. That indicates differences in the electronic structure and and it can be deduced that rGO is more metallic and therefore it has better conductivity.

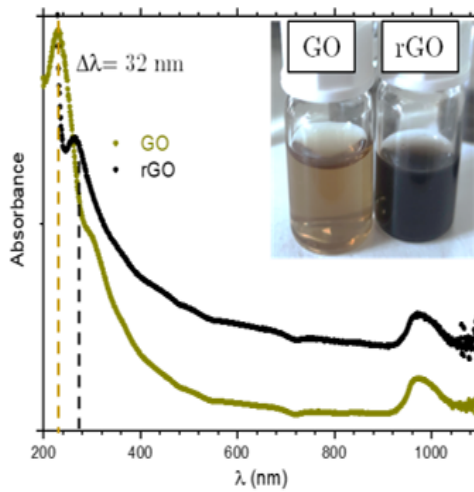


Figure 2: Absorbance per wavelength  $\lambda$ (nm) of GO and rGO. Image courtesy of Elisa Palacios Lidón.

GO is an electronically hybrid material that presents both conducting  $\pi$ -states from the hybridized  $p_z$  orbitals of the  $sp^2$  hybridisation and a sizeable energy gap between the  $\sigma$ -

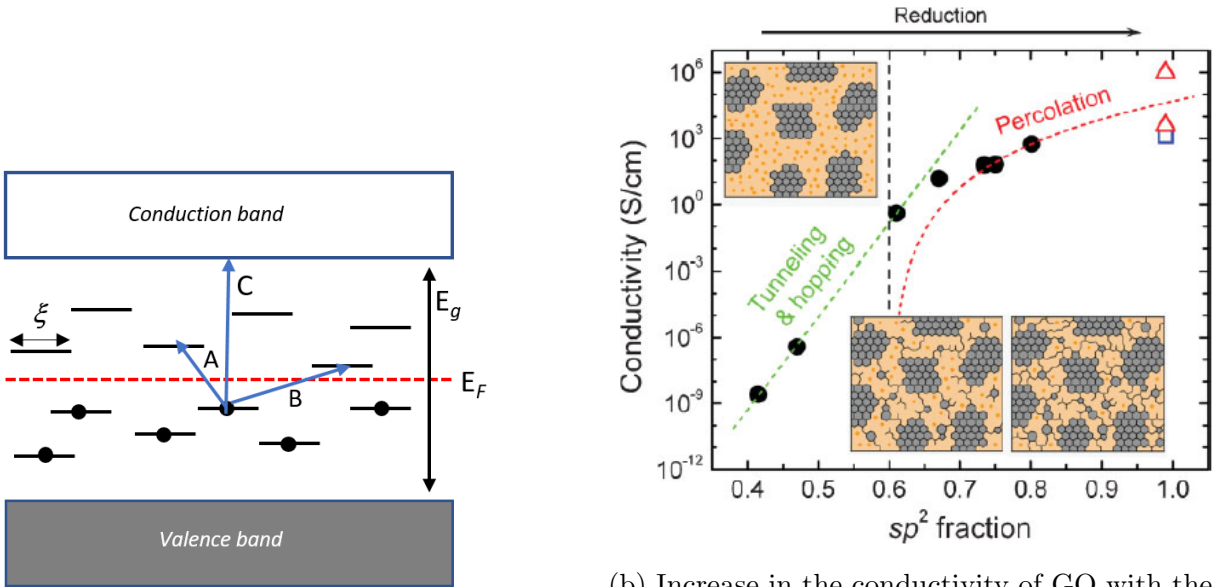
states of the carbon atoms with  $sp^3$  hybridisation [5]. Due to the random distribution of the different oxygen-containing functional groups in the basal plane, small regions with  $sp^2$  or  $sp^3$  are formed. In addition, in disordered materials each site possesses a unique environment and electrons may exhibit a preference for specific locations within the material. As a result, the electronic wave functions become localized in space, exhibiting a characteristic localization length,  $\xi$ . At finite temperature, conductivity is achieved through the assistance of phonons, which facilitate the tunneling or hopping of electrons between these localized states. Then, the probability of an electron transitioning or hopping from one state to another, with an energy increase of  $\Delta E_{i,j}$ , is directly related to the probability of encountering a phonon with that specific energy  $\propto \exp(-\Delta E_{i,j}/kT)$ . Moreover, the probability of the transition also relies on the overlap between the states involved, which is exponentially affected by the distance  $r_{i,j}$  separating them. The transition rate between states can be express, according to [8], as follows:

$$\Gamma_{i,j} \propto \exp\left(-\frac{\Delta E_{i,j}}{kt}\right) \exp\left(-\frac{2r_{i,j}}{\xi}\right) \quad (1)$$

where the initial exponential factor corresponds to the count of phonons with an energy of  $\Delta E_{i,j}$ , while the second factor exposes the square of the transition matrix element, as prescribed by the golden rule.

Two significant conclusions can be drawn from (1): Firstly, the rates follow an exponential distribution, hence percolation approaches are suitable. Secondly, the energy difference and spatial separation have comparable impacts, indicating a trade-off between them [8].

The energy gap in GO depends directly on the fraction of  $sp^2/sp^3$  hybridized domains [9]. It is possible to tune the ratio of  $sp^2/sp^3$  to convert GO from an insulator to a semiconductor [5]. To decrease the difference between the energy states and, thus, reduce the energy gap for some technological applications, the solution is to use rGO by removing the functional groups, in such a way that the hops of the electrons from one region to another of the material are more likely, thus, increasing the conductivity. New  $sp^2$  clusters are created when GO is reduced, which allows percolation pathways between the  $sp^2$  domains. Thus, these  $sp^2$  states facilitate electronic transport by hopping [5].



(a) Schematic representation of electrons energy states in GO. Image adapted from [8].

(b) Increase in the conductivity of GO with the reduction of functional groups and, therefore, the increment of the  $sp^2$  fraction. Adapted from [1].

Figure 3: Schematic representation of electrons energy states in GO and increase in conductivity of GO with the increase in  $sp^2$  fraction and the degree of reduction.

In Fig. 3 (a), the energy states of the electrons in GO are illustrated, where  $E_g$  is the gap energy from the valence band to the conduction band and  $E_F$  is the Fermi energy.

It can be shown in Fig. 3 (b), how the conductivity increases with the  $sp^2$  fraction, and how it changes from charge transport by hopping to transport by percolation.

## 2.4 Applications of GO and rGO.

GO and rGO can be used for a wide range of applications in many fields, because of the tunability of its properties depending on the extent of reduction.

### Transparent conductors with rGO.

Since rGO is atomically thin, it is almost transparent in the visible spectrum. From an electronic point of view, it behaves like a semimetal, displaying a finite density of states at the Fermi level and manifesting small changes in electrical conductance with gate voltage in field-effect devices. Hence, rGO is a potential candidate to replace indium tin oxide (ITO) for transparent conductor applications in several devices that require

electrochemical stability and mechanical flexibility, such as displays, organic light-emitting diodes, and organic solar cells [5].

### **Gas sensing.**

GO is very useful for gas sensing applications because of its oxygen-containing functional groups, its electronical features and its high surface to volume ratio. It can detect gases at room temperature (RT), something that is not possible with conventional devices. It is also possible to fabricate sensors on flexible substrates with GO and rGO [10].

GO reveals a really fast response to changes in relative humidity (RH), with a detection time as fast as 30 milliseconds near RT, making it an excellent material for sensing RH variations. The sensitivity of GO to RH arises from its dielectric constant, which increases as the RH increases [10].

The relative resistance of GO can be used for the detection of gases such as NO<sub>2</sub> and SO<sub>2</sub> at RT, due to oxygen-containing functional groups, because it is independent on the RH values, hence, devices like that can be used under any atmospheric conditions [10].

For some gases, the detection capabilities of rGO are improved compared to those of GO due to its substantially improved conductivity and retention of some of the oxygen-containing functional groups. It can detect hazardous gases such as CO<sub>2</sub> and NO [10].

### **Biological applications of GO and rGO.**

The fluorescence of GO can be tuned between NIR, visible and ultraviolet, so this suggests its suitability for numerous biomedical applications. Some notable applications of GO in biomedicine include live cell imaging, cancer treatment, biosensing, and drug delivery. For instance, GO functionalized with polyethylene glycol (PEG) can be used for delivery of water-insoluble anticancer drugs, benefiting from its hydrophilic nature and excellent solubility in water. Furthermore in an experiment with mice, PEGylated GO has been applied to photothermal therapy, because of the optical absorbance of GO in the NIR region. Remarkably, intravenous administration of PEGylated GO followed by low-power NIR laser irradiation resulted in highly effective tumor ablation without any observable toxic effects [6, 5].

GO can be used for gene delivery, a technique employed to introduce DNA into cells for the treatment of various genetic disorders, because its functional groups allows it to combine with a variety of biomolecules and polymers. Besides, GO also plays an important role in bone and tissue engineering [6].

GO also finds application as a broadband optical limiter, because of its singular nonlinear optical characteristics. Moreover, GO can be combined with complementary nonlinear optical materials, to improve its optical limiting properties [5].

## 3 Surface physics and Atomic Force Microscopy.

### 3.1 Work function of a solid and surface potential.

The work function of a solid represents the minimum energy needed to extract an electron from the interior of the solid and bring it to a point in a vacuum [11]. The work function of a solid is composed of two different contributions: One of them is the work necessary to carry an electron from the interior of the solid to the surface and the other contribution is the work necessary for the electron to pass through the surface and reach a point in vacuum without being influenced by the ions of the solid.

To begin with, the first contribution to the work function, which is the energy necessary to move an electron from the interior of the solid to the surface, is equal to the Fermi energy,  $\varepsilon_F$ , which represents the highest energy level occupied by the electrons in the solid. The second contribution arises from the perturbation in the charge distribution near the surface, which can be described by the "jellium model." This model assumes a uniform positive charge density throughout the material, except at the surface, where it abruptly goes to zero [12]. At the surface, there is a discontinuity in charge distribution, causing electrons to generate an electron density that follows the surface shape [13]. This generates a barrier that electrons near the surface can overcome through tunneling. The electronic density in this model can be represented like it is shown in Fig. 4.

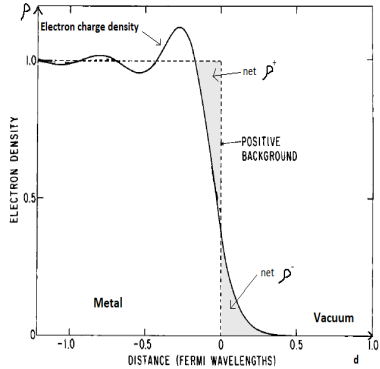


Figure 4: Charge distribution of the positive ions (dashed line) and electron density (solid line) vs. distance  $x$  normal to the surface. Adapted from [13].

As depicted in Fig. 4, the superposition of the postive charge density and the electron density taking into account the tunneling effect, results in the emergence of a surface density of dipoles, with positive charge density,  $\rho^+$ , near the inner surface and negative charge density,  $\rho^-$ , near the outer surface, which creates an electric field that acts as a barrier, preventing the electrons from escaping the solid. The energy required to overcome this barrier is the second component of the work function and can be expressed as  $\phi = -eV_s$ , where  $e$  represents the charge of an electron and  $V_s$  represents the electrostatic potential associated with the surface density of dipoles.

Hence, the work function can be expressed as follows:

$$W = \varepsilon_F + \phi \quad (2)$$

The behavior of the work function of two metals, A and B, plays a crucial role in understanding atomic force microscopy (AFM). When these metals are isolated, each has its own unique work function, so the Fermi level and the energy required to traverse the surface will be different for each metal, as represented in Fig. 5 (a). Nevertheless, when they are brought into close proximity and electrically connected, electrons can flow from the metal with lower work function to the one with higher work function through tunneling, as illustrated in Fig. 5 (b). This leads to a surface charge formation, generating an electrostatic potential and intense electric fields. The system reaches equilibrium when the Fermi levels of the two metals are equal, which occurs when  $U_{SP} = eV_{SP} = \Delta\phi$ ,

where  $V_{SP}$  is the surface potential between the two metals, which includes the contact potential, isolated charges, dipoles, among other types of electromagnetic interactions. This is represented in Fig. 5 (c).

Applying an external voltage  $V_{bias}$ , that satisfies  $V_{bias} = -V_{SP}$ , modifies the entire band structure, resulting in the elimination of the electric field between the metals, as represented in Fig. 5 (d). Knowing the work function of one metal, the work function of the other metal can be determined using  $V_{SP} = \Delta\phi/e$ .

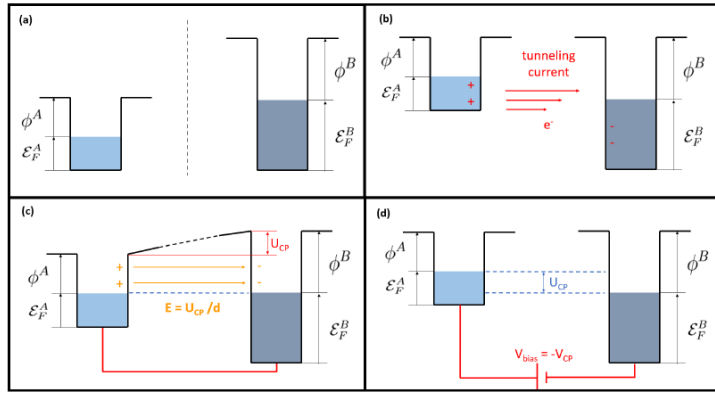


Figure 5: (a) Representation of the work function of each metal A and B, when they are isolated. (b) Electrical contact established through tunneling current. (c) Equilibrium attained between the two metals. (d) External voltage equal to surface potential. Adapted from TFG of Eva Osuna.

### 3.2 The fundamentals of the Atomic Force Microscope (AFM).

The Atomic Force Microscope (AFM) is an advanced microscope that operates by detecting the forces between a tiny probe (the tip) and the surface of a sample. Unlike traditional optical microscopes, AFM overcomes the limitations imposed by optical diffraction. It offers exceptional imaging capabilities, allowing for the visualization of a wide range of surfaces with remarkable detail at the nanoscale level. In Fig. 6, the fundamental assembly of an AFM with its basic components is illustrated.

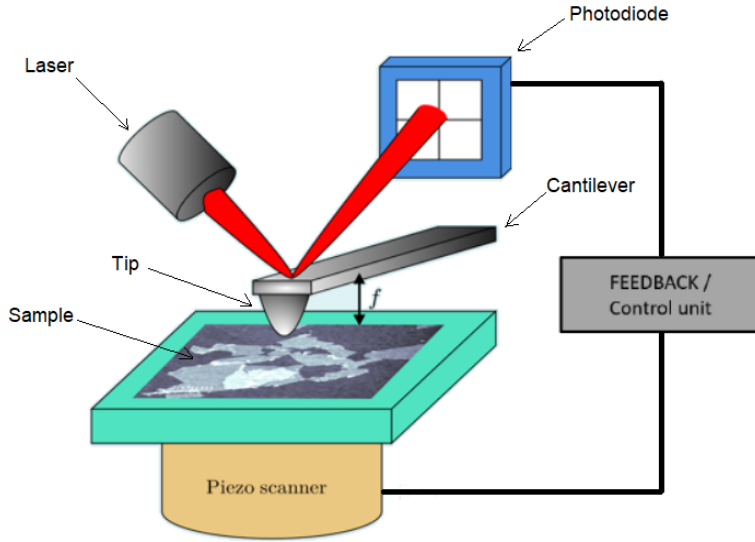


Figure 6: Fundamental elements of an AFM. Image courtesy of Mario Navarro.

The AFM is made up of the following parts: Tip, which is the probe that interacts with the sample; cantilever, which deflects due to the forces of interaction between the tip and the sample, allowing the measurement of those forces; laser, which makes it possible to detect small deflections of the micro-lever in a simple and very sensitive way, since it deviates its trajectory; four panel photodiode, which measures the deviation of the laser pulse, very accurate, providing quantifiable information to generate the image; piezoelectric, which is the displacement system that allows the tip-sample distance to be varied with great precision and to move one relative to the other in the direction of the sample plane to scan the image; control unit, which records the interactions and, finally, feedback system, which maintains constant a measurable physical interaction between the tip and sample.

AFM can operate in static or dynamic modes to measure the bending or vibrational properties of the cantilever, respectively. In contact mode, the tip-sample distance is controlled to keep a constant cantilever bending. In the dynamic modes, variations in the vibrational behavior of the cantilever caused by interactions between the tip and the sample are detected, involving parameters such as resonant frequency and oscillation amplitude [14].

In this work, a dynamic and non-contact mode was employed, where the cantilever is stimulated by a piezoactuator to oscillate at its resonant frequency. Interactions between

the tip and sample induce deflection and torsion of the cantilever. To detect these interactions, a laser beam is directed onto the back of the cantilever. The deflection of the cantilever alters the path of the laser beam, and this deviation is measured by a four-panel photodiode, indicating the changes in the oscillation amplitude and resonant frequency of the cantilever [14].

The employed technique in this work is the Non-Contact - Amplitude Modulation - Dynamic Scanning Force Microscopy (NC-AM-DSFM) mode. In this mode, the surface is scanned, to obtain images, using the tip while keeping the oscillation amplitude constant. This is achieved through a control circuit that includes a control unit which records the interactions and a feedback system to maintain the desired oscillation amplitude [14]. To avoid touching the surface in this mode, the oscillation amplitude has to be relatively small  $\sim 1 - 5$  nm approx. Besides, the sample tip distance has to be large enough to avoid entering the repulsive part of the interaction potential during the closest approach point of the oscillation.

### 3.3 Kelvin Probe Force Microscopy (KPFM).

In AFM, various forces such as Van der Waals, electrostatic, magnetic, capillary, forces in liquids (adhesion), or Fermi repulsion can contribute to the total force between the tip and the sample. Differentiating the individual contributions of these interactions poses a challenge in AFM measurements. To address this, several experimental techniques have been developed to selectively isolate specific interactions. As the electrical properties of GO are studied in this work, the technique called Kelvin Probe Force Microscopy (KPFM) has been used, which focuses on isolating and characterizing the electrostatic interaction [14].

The electrostatic energy of a continuous charge distribution can be expressed according to [15], in the form:

$$W_{elec} = -\frac{\epsilon_0}{2} \int E^2 dv \quad (3)$$

where  $E$  is the electric field,  $\epsilon_0$  is the vacuum permittivity and  $dv$  is a volume element.

For a flat-parallel capacitor, where two metal plates of surface A are positioned at a distance  $d$ , the electric field ( $E$ ) generated by applying a potential difference ( $V$ ) between the plates is constant throughout the capacitor. The electrostatic energy stored in the capacitor can be expressed as follows:

$$W_{elec} = -\frac{1}{2}QV = -\frac{1}{2}C(d)V^2 \quad (4)$$

where  $C = \epsilon_0 A/d$  is the capacity of the capacitor.

The tip-sample system can be described as a capacitor with a complex geometry, resulting in an electrostatic energy given by the following equation:

$$W_{elec} = -\frac{1}{2}C(z, \xi)V^2 \quad (5)$$

where  $V$  is the tip-sample voltage difference and  $C(z, \xi)$  is the capacity, which depends on the tip-sample distance  $z$  and the geometry of the tip  $\xi$ .

The force is given by:

$$F_{elec} = -\frac{\partial W_{elec}}{\partial z} = \frac{1}{2} \frac{\partial C(z, \xi)}{\partial z} (V_{bias} - V_{SP})^2 \quad (6)$$

The voltage difference between the tip and sample is induced by the surface potential  $V_{SP}$ . So, to minimize the electrostatic energy, an external voltage,  $V_{bias}$ , can be applied in a way that makes  $V_{bias} = -V_{SP}$ . These concepts and their relationship were previously discussed in Section 3.1. However, this force experienced by the tip translates into a very slight deflection of the cantilever that is difficult to detect for small potential differences, therefore, what is done to solve this is to apply a potential difference between the tip and the sample of the form  $V_{DC} + V_{AC} \sin(\omega_{elec}t)$ , which enables the electrostatic interaction to be divided into three components:

$$\begin{aligned}
F_{elec} &= \frac{1}{2} \frac{\partial C(z, \xi)}{\partial z} (V_{bias} - V_{SP})^2 = \frac{1}{2} \frac{\partial C(z, \xi)}{\partial z} (V_{DC} + V_{ac} \sin(\omega t) - V_{SP})^2 \\
&= \underbrace{\frac{\partial C(z, \xi)}{\partial z} \left[ \frac{V_{ac}^2}{4} + \frac{1}{2}(V_{DC} - V_{SP})^2 \right]}_{F_{DC}} + \underbrace{\frac{\partial C(z, \xi)}{\partial z} (V_{DC} - V_{SP}) V_{ac} \sin(\omega t)}_{F_\omega} \\
&\quad - \underbrace{\frac{\partial C(z, \xi)}{\partial z} \frac{V_{ac}^2}{4} \cos(2\omega t)}_{F_{2\omega}}
\end{aligned} \tag{7}$$

So, the electrostatic force can be expressed as a function of the harmonic components of electrostatic interaction.

In this research, the frequency shift of the tip oscillation due to the interaction was utilized, instead of directly measuring the force to perform Kelvin Probe Force Microscopy (KPFM). When the oscillations are small, the alteration in the linear resonance frequency, denoted as  $f_0 = \omega_0/(2\pi)$ , due to the electrostatic interaction can be described as follows:

$$\begin{aligned}
\Delta f &= -\frac{f_0}{2k_{cantilever}} \frac{\partial F_{elec}}{\partial z} = -\frac{f_0}{4k_{cantilever}} \frac{\partial^2 C(z, \xi)}{\partial z^2} (V_{bias} - V_{SP})^2 \\
&= -\frac{f_0}{4k_{cantilever}} \frac{\partial^2 C(z, \xi)}{\partial z^2} (V_{DC} + V_{ac} \sin(\omega t) - V_{SP})^2 \\
&= -\underbrace{\frac{f_0}{2k_{cantilever}} \frac{\partial^2 C(z, \xi)}{\partial z^2} \left[ \frac{V_{ac}^2}{4} + \frac{1}{2}(V_{DC} - V_{SP})^2 \right]}_{\Delta f_{DC}} \\
&\quad - \underbrace{\frac{f_0}{2k_{cantilever}} \frac{\partial^2 C(z, \xi)}{\partial z^2} (V_{DC} - V_{SP}) V_{ac} \sin(\omega t)}_{\Delta f_\omega} + \underbrace{\frac{f_0}{2k_{cantilever}} \frac{\partial^2 C(z, \xi)}{\partial z^2} \frac{V_{ac}^2}{4} \cos(2\omega t)}_{\Delta f_{2\omega}}
\end{aligned} \tag{8}$$

where  $k_{cantilever}$  is the elastic constant of the cantilever.

We use a lock-in amplifier to extract the first,  $\omega$ , and second,  $2\omega$ , harmonic components. The first harmonic signal is utilized to provide feedback that nullifies the signal by adjusting  $V_{DC} = -V_{SP}$  at every point. This approach enables the acquisition of surface potential ( $V_{SP}$ ) images. Moreover, the second harmonic provides valuable information

about the tip-sample capacitance.

## 4 Experimental results.

### 4.1 Preparation of the sample.

The substrate used for this work was 300 nm thick SiO<sub>2</sub> grown on highly doped p-type Silicon (Boron). The sample preparation process is as follows: First, the silicon oxide surface is cleaned with ethanol to remove organic impurities and then rinsed with Milli-Q-type deionized ultrapure water. Once the substrate is clean, it is treated with a UV/Ozone for about 15 minutes to recover the hydrophilicity of the substrate. Subsequently, the material of interest, whether it be GO or rGO, is deposited by drop casting from the solutions onto the substrate. After the drop dries, it is delicately washed again with ultrapure water to remove possible residual impurities present in the solution.

rGO solutions are prepared by adding hydrazine hydrate (50-60%) to the GO water suspension and allowing it to react for as long as needed to set the degree of rGO reduction. It is crucial to maintain a low concentration of the solutions in order to obtain individual rGO flakes.

### 4.2 Monolayer GO on SiO<sub>2</sub> substrate.

To analyze the structural and electrical properties of GO, images of GO individual monolayer flakes deposited on a 300 nm silicon oxide (SiO<sub>2</sub>) thermally grown on silicon substrate were acquired.

#### 4.2.1 Topography and KPFM of monolayer GO

Fig. 7 (a) depicts the topography of a GO monolayer flake. The accompanying graph on the right displays a profile of the sample taken from left to right along the gray line in the left image, representing the height of the GO layer. The average height of the layer is approximately 2 nm, with a maximum of 2.5 nm and a minimum close to 1.5 nm.

Fig. 7 (c) illustrates the corresponding KPFM (Kelvin Probe Force Microscopy) image.

The graph attached to the right shows a profile along the green line in the left image, from top to bottom, to achieve precise quantitative values of the surface potential of the GO sample.

As previously mentioned, KPFM measures the surface potential between the tip and the sample, which represents the contact potential and the localized charge distribution. The surface potential is observed to vary between different regions, which may suggest the presence of localized charge domains, due to the disordered arrangement of the GO functional groups. What indicates that they are charges is that if the same GO flake is measured for hours, a potential variation is seen in the different zones using KPFM. This variation is due to the movement of the charges in the material by hopping between the closest zones. Therefore, it is being seen that the KPFM image corresponds to the observation of localized charge domains. It can be seen that the maximum potential difference between two zones is close to 2.1 V.

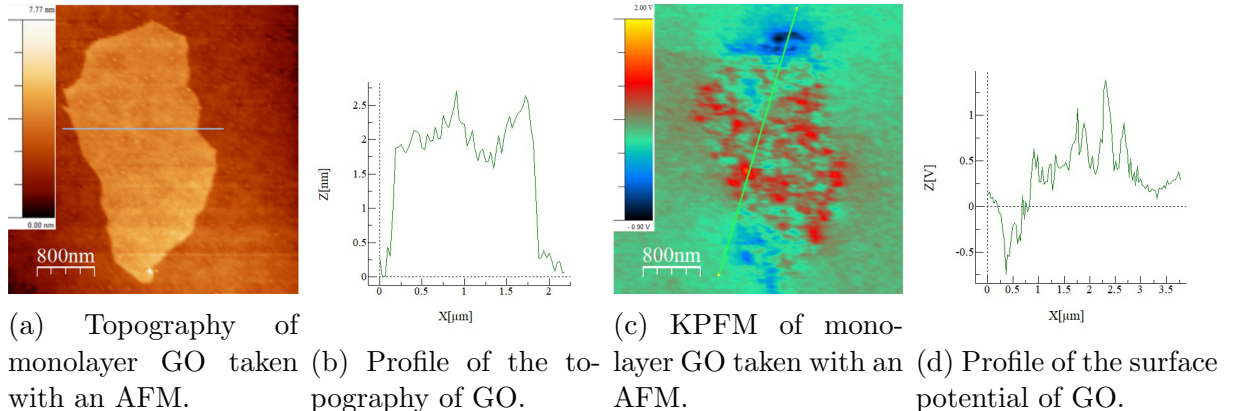


Figure 7: Topography and KPFM of monolayer GO and the profile taken along the green line.

### 4.3 Flakes of rGO on SiO<sub>2</sub> substrate.

#### 4.3.1 Topography and KPFM of rGO flakes.

Figure 8 (a) shows the topography of several rGO flakes, that were reduced for two days at room temperature. On the center of the large single flake, there is a superposition of two and three flakes. The accompanying graph on the right presents a profile of the sample, taken from left to right along the green line in the left image, representing the

height of the rGO layers. The average height of a single layer is approximately 2.5 nm, while the double layer has a total height of 4 nm. It should be noted that stacked layers do not simply add the heights of the individual layers.

Figure 8 (c) depicts the KPFM measurement of rGO flakes, corresponding to the topography displayed in (a). The graph attached to the right shows a profile along the green line in the left image, from left to right, which collects precise quantitative values of the surface potential of the rGO sample.

The surface potential, obtained by KPFM, exhibits a relatively more homogeneous spatial distribution throughout the rGO layer. This enhanced homogeneity of charge distribution, compared to GO, is due to the fact that many functional groups have been eliminated and the  $sp^2$  fraction is increased, therefore it conducts more and the dynamics of the electrons is faster, finally seeing an average. As a consequence, of the larger conductivity of rGO compared to the GO one, the localization length,  $\xi$ , increases facilitating an easier conduction through electronic hopping. As mentioned in section 2.3, when rGO is very reduced and the fraction of  $sp^2$  is greater than 0.6, the conduction mechanism is by percolation, instead of hopping, so charges move much faster in the material.

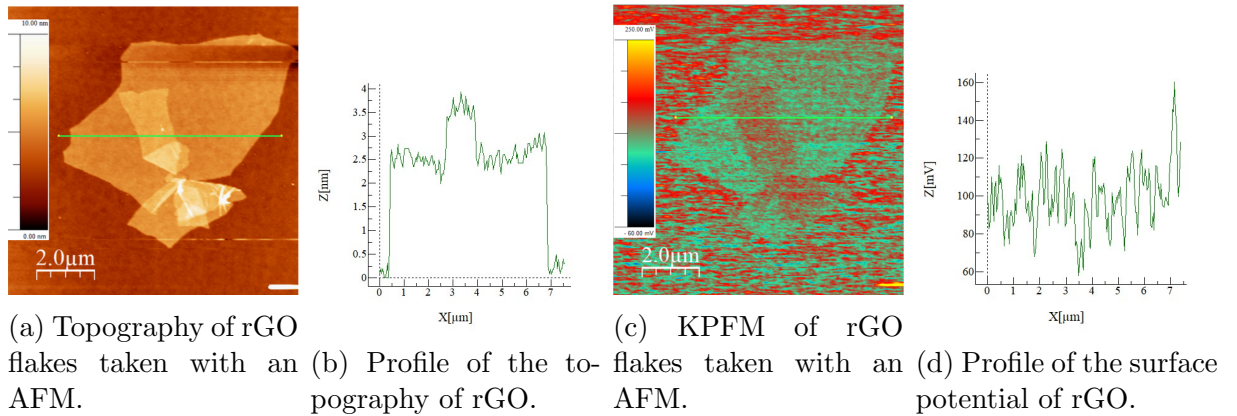


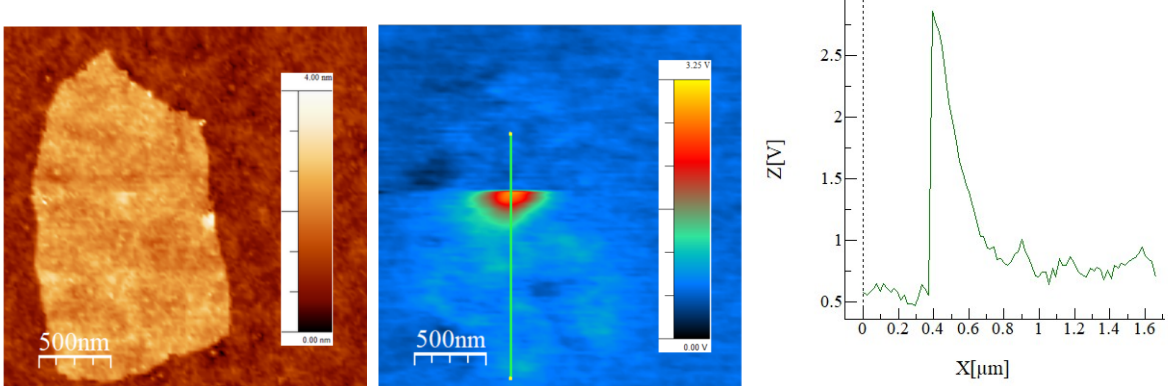
Figure 8: Topography and KPFM of rGO flakes and the profile taken along the green line.

#### 4.4 Charge injection.

Figure 9 (a) depicts the topography of GO monolayer. In Fig. 9 (b), it is represented the KPFM image of the GO monolayer, corresponding to the topography displayed in (a). To

make this image and observe the speed of propagation of the charge in GO, we begin to scan with KPFM, in a typical way, that is, in horizontal lines with round trips. Then, at one point, the tip is placed on the sample, for approximately 30 ms, to produce an electric discharge and, immediately, the measurement is continued to observe the propagation of the charge in the material. In this way, it can be verified if the material is a better or worse conductor, since if the charge propagates rapidly, the material will be a good conductor, while slower propagation suggests poorer conductivity.

The graph in Fig. 9 (c) shows a profile along the green line in (b), from top to bottom, which collects precise quantitative values of the surface potential of the GO sample. In this graph, it can be seen that the charge is highly concentrated in a small region and has barely spread in the GO during the image acquisition. This observation agrees with the information exposed in section 2.3, where it was explained that conduction by hopping is not efficient in GO, due to the substantial separation between localized electronic states in the gap, as shown in figure 3. So, because of the insulating nature of the material, the charge is distributed in times comparable to the acquisition time of a line and, therefore, the decay of the charge can be monitored.



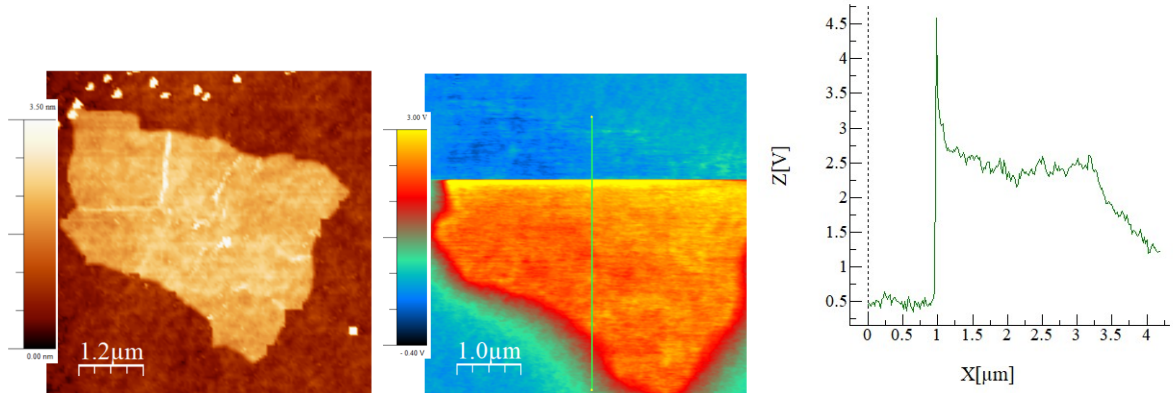
(a) Topography of GO taken with an AFM. (b) KPFM of GO taken with an AFM. (c) Profile of the surface potential of GO.

Figure 9: Topography and KPFM of GO in charge injection experiment and the profile taken on the green line.

Figure 10 (a) shows the topography of rGO monolayer. Figure 10 (b) illustrates the KPFM measurement of the rGO monolayer, corresponding to the topography displayed

in (a). The captured image represents the moment immediately after the application of an electrical discharge to the rGO, to assess the speed at which the charge propagates.

The accompanying graph on Fig. 10 (c) represents a profile along the green line in the left image, from top to bottom. In this figure, it can be seen that the charge has spread rapidly throughout the rGO, much faster than the acquisition time. This observation is consistent with the explanation provided in section 2.3. The removal of functional groups, which are not arranged uniformly, results in the formation of isolated  $sp^2$ -bonded domains, which create pathways for charge percolation. Consequently, the conduction in rGO is good for electronic devices. So, with this charge injection experiment in GO and rGO, it has been possible to observe how by reducing GO, the conductivity of the material increases. In rGO, the charge reaches the equilibrium configuration much faster than the acquisition time of the surface potential.

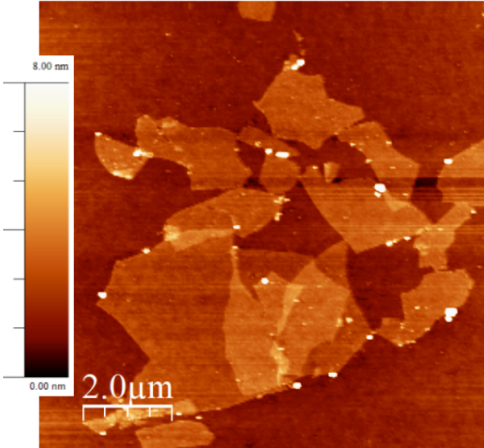


(a) Topography of rGO taken with an AFM. (b) KPFM of rGO taken with an AFM. (c) Profile of the surface potential of rGO.

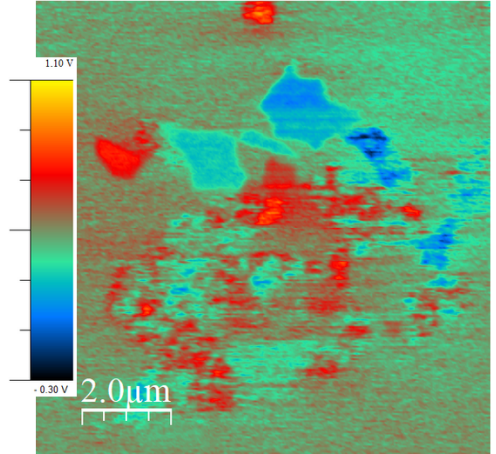
Figure 10: Topography and KPFM of rGO and the profile taken on the green line.

#### 4.5 Comparison GO and rGO on $\text{SiO}_2$ substrate.

In this section, the GO and rGO flakes co-deposited on the substrate will be identified, in addition, their properties will be compared, based on the characteristic information obtained from each one in the previous sections.



(a) Topography of mix GO and rGO taken with an AFM.



(b) KPFM of mix of GO and rGO taken with an AFM.

Figure 11: Topography and KPFM of mix GO and rGO and the profile taken on the green line.

Figure 11 (a) shows the topography of several GO and rGO flakes. With this image it is not possible to distinguish GO from rGO, however with the KPFM representation in (b), they can be distinguished taking into account the charge distribution for each material according to their individual images in figures 7 and 8. The flakes with a more uniform potential are made of rGO, while the flakes that show a heterogeneous charge distribution are made of GO.

It can be observed in figure 11 (b) that two flakes of rGO that touch each other adopt the same potential, because the charge easily moves between them, due to its conductive nature, to find the equilibrium configuration. However, if two flakes of rGO are separated by one of GO, then they cannot reach that equilibrium configuration, due to the insulating character of GO, which does not allow the fluid movement of charges.

Besides, since they are supported on an insulating substrate, they do not have a well-defined potential reference and, therefore, the surface potential measured on rGO flakes is affected by their local environment. For example, the bottom left flake is from rGO and is hardly different from the substrate in KPFM.

## 5 Conclusions and future.

In conclusion, in this work it has been possible to verify experimentally, by means of an AFM with the KPFM technique, how the charges are distributed in GO, presenting the existence of localized charge domains in a non-uniform way due to the fact that it is a disordered material with functionalization groups arranged randomly. That is, the nanoscale charge density has been measured in GO.

It has also been verified, how this charge distribution observed in GO changes when it is reduced, obtaining rGO. The observed surface potential in rGO is uniform, indicating that conduction is increased, as one sees an average of the much faster electron dynamics.

This increase in conduction by reducing GO has been verified experimentally, using the charge injection experiment. In this experiment, it has been observed that the charge propagates much faster in rGO than in GO, indicating that the localization length increases with the fraction of  $sp^2$ , facilitating hopping conduction, and even changing the conduction mechanism by hopping to conduction by percolation.

Once their individual electrical properties are known, they can be distinguished in a sample with flakes of both, as well as understanding and explaining their behavior, based on the insulating nature of GO and the conductive nature of rGO.

There is still a lot of study on the electrical properties of GO and rGO, such as capacity, which can be studied with KPFM, using the  $2\omega$  signal. The study of these properties could lead to performance optimization of GO and rGO based devices.

The future applications of GO and rGO are very varied, because their properties can be modified to adapt them to a specific application, achieving very different properties, eliminating different functional groups (hydroxil, epoxy,...). For example, GO is hydrophilic and insulating, however rGO, quite small, is hydrophobic and semiconducting. Another quality is its ability to interact, through its functional groups, with other compounds.

## References

- [1] G. Eda and M. Chhowalla, “Chemically derived graphene oxide: towards large-area thin-film electronics and optoelectronics,” *Advanced materials*, vol. 22, no. 22, pp. 2392–2415, 2010.
- [2] K. S. Novoselov, A. K. Geim, S. V. Morozov, D.-e. Jiang, Y. Zhang, S. V. Dubonos, I. V. Grigorieva, and A. A. Firsov, “Electric field effect in atomically thin carbon films,” *science*, vol. 306, no. 5696, pp. 666–669, 2004.
- [3] G. Yang, L. Li, W. B. Lee, and M. C. Ng, “Structure of graphene and its disorders: a review,” *Science and technology of advanced materials*, vol. 19, no. 1, pp. 613–648, 2018.
- [4] G. Gui, J. Li, and J. Zhong, “Band structure engineering of graphene by strain: First-principles calculations,” *Physical Review B*, vol. 78, no. 7, p. 075435, 2008.
- [5] K. P. Loh, Q. Bao, G. Eda, and M. Chhowalla, “Graphene oxide as a chemically tunable platform for optical applications,” *Nature chemistry*, vol. 2, no. 12, pp. 1015–1024, 2010.
- [6] S. Priyadarsini, S. Mohanty, S. Mukherjee, S. Basu, and M. Mishra, “Graphene and graphene oxide as nanomaterials for medicine and biology application,” *Journal of Nanostructure in Chemistry*, vol. 8, pp. 123–137, 2018.
- [7] V. Agarwal and P. B. Zetterlund, “Strategies for reduction of graphene oxide—a comprehensive review,” *Chemical Engineering Journal*, vol. 405, p. 127018, 2021.
- [8] M. Pollak, M. Ortúñ, and A. Frydman, *The electron glass*. Cambridge University Press, 2013.
- [9] A. Mathkar, D. Tozier, P. Cox, P. Ong, C. Galande, K. Balakrishnan, A. Leela Mohana Reddy, and P. M. Ajayan, “Controlled, stepwise reduction and band gap manipulation of graphene oxide,” *The journal of physical chemistry letters*, vol. 3, no. 8, pp. 986–991, 2012.

- [10] M. Donarelli and L. Ottaviano, “2d materials for gas sensing applications: a review on graphene oxide, mos<sub>2</sub>, ws<sub>2</sub> and phosphorene,” *Sensors*, vol. 18, no. 11, p. 3638, 2018.
- [11] N. W. Ashcroft and N. D. Mermin, *Solid state physics*. Cengage Learning, 2022.
- [12] M. Brack, “The physics of simple metal clusters: self-consistent jellium model and semiclassical approaches,” *Reviews of modern physics*, vol. 65, no. 3, p. 677, 1993.
- [13] N. D. Lang, “The density-functional formalism and the electronic structure of metal surfaces,” in *Solid State Physics*, vol. 28, pp. 225–300, Elsevier, 1974.
- [14] E. Meyer, H. J. Hug, R. Bennewitz, *et al.*, *Scanning probe microscopy*, vol. 4. Springer, 2003.
- [15] J. D. Jackson, *Classical electrodynamics; 2nd ed.* New York, NY: Wiley, 1975.

## **Appendix**

The modality of this final degree project is for initiation into research.